Engineering the Spin–Flip Limited Exciton Dephasing in Colloidal CdSe/CdS Quantum Dots

Nicolò Accanto,[†,‡] Francesco Masia,[†,‡] Iwan Moreels,[§,⊥,∥] Zeger Hens,[§] Wolfgang Langbein,[†] and Paola Borri*[,†,‡]

[†]School of Physics and Astronomy, Cardiff University, The Parade, Cardiff CF24 3AA, United Kingdom, [‡]School of Biosciences, Cardiff University, Museum Avenue, Cardiff CF10 3AX, United Kingdom, [§]Physics and Chemistry of Nanostructures and Centre for Nano and Biophotonics, Ghent University, Ghent B-9000, Belgium, and [⊥]IBM Research-Zürich, Säumerstrasse 4, CH- 8803 Rüschlikon, Switzerland. [∥]Present address: Istituto Italiano di Tecnologia, Via Morego 30, IT-16163 Genova, Italy.

ABSTRACT

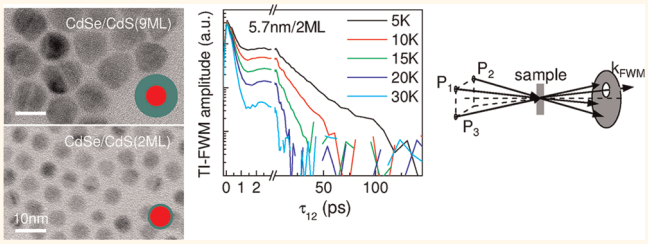

We have measured the intrinsic exciton dephasing in high-quality zinc blende CdSe/CdS colloidal quantum dots in the temperature range from 5 to 170 K using a sensitive three-beam photon echo technique in heterodyne detection, which is not affected by spectral diffusion. Pure dephasing *via* acoustic phonons dominates the initial dynamics, followed by an exponential zero-phonon line dephasing. From the temperature dependence of the zero-phonon line dephasing, the exciton lifetime, and the exciton thermalization within its fine structure, we show that the zero-phonon line dephasing of the lowest bright state originates from the phonon-assisted spin–flip to dark exciton states. Importantly, we can control the dephasing by tailoring the exciton fine structure through its dependence on the dot core size and shell thickness, as expected from the spin–flip mechanism. By reducing the electron–hole exchange interaction with increasing core size and delocalization of the electron wave function in the quasi-type-II core/shell band alignment, we find the longest zero-phonon line dephasing time of ∼110 ps at 5 K in dots with the largest core diameter (5.7 nm) and the thickest CdSe shell (9 monolayers) in the series studied.

KEYWORDS: exciton dephasing · transient four-wave mixing · colloidal nanocystals

Coherent quantum dynamics of excitons in semiconductor quantum dots (QDs) are of key interest, besides fundamental physics, for many applications ranging from quantum computing[1] to advanced photonics devices including single-photon switches[2] and thresholdless nanolasers.[3] Extensive work has been reported on this topic, investigating almost exclusively epitaxially grown QDs which are embedded in a matched defect-free crystalline environment. With the recent advances in colloidal synthesis, high-quality semiconductor nanocrystals have become more and more available,[4] with the advantage of being much less expensive to fabricate and easier to engineer with a large variety of sizes, shapes, and composition.

After the first pioneering works[5,6] in the early 2000s, it is now well understood that the exciton decoherence in semiconductor quantum dots is non-exponential even at low temperatures, corresponding to a non-Lorentzian homogeneous line shape with a sharp zero-phonon line (ZPL) superimposed onto a broad acoustic phonon band. Importantly, it was shown that in epitaxially grown InAs/GaAs QDs the ZPL dephasing is limited at 5 K by the ∼1 ns radiative lifetime.[7,8] The picture is much less clear for colloidal QDs which have smaller sizes and stronger dielectric confinement and, in turn, longer radiative lifetimes. While a ZPL ∼ 10 μeV was reported in large core wurtzite CdSe/ZnS colloidal QDs at low temperature *via* spectral hole burning[9] and single-dot spectroscopy experiments[10] (corresponding to ∼100 ps exciton dephasing time much shorter than the ∼10 ns radiative lifetime), its physical origin remained an open question, also because these experiments were limited by spectral diffusion (a variation of the QD transition frequency over time from slow fluctuations of the QD environment).

We recently measured the temperature-dependent ZPL dephasing of the lowest bright exciton in large core (∼8 nm) CdSe/ZnS wurtzite QDs using a sensitive three-beam four-wave mixing (FWM) photon echo technique unaffected by spectral diffusion.[11] We compared the dephasing time with the exciton density dynamics within

* Address correspondence to borrip@cardiff.ac.uk.

Received for review March 6, 2012 and accepted May 7, 2012.

Published online May 07, 2012
10.1021/nn300992a

the exciton fine structure measured in the same experiment. Our results showed unambiguously that the physical origin of the zero-phonon line dephasing at 5 K is the rapid (~100 ps) phonon-assisted spin−flip from the lowest bright state to the dark exciton state. This finding is different from InGaAs/GaAs epitaxially grown QDs, where the bright−dark exciton relaxation is in the 10−100 ns range, longer than the ~1 ns radiative lifetime.[7] Besides differences in the bulk material parameters, one can argue that the reason for the longer spin−flip time in epitaxially grown InAs/GaAs QDs is the smaller fine structure splitting energy Δ_{BD} between the lowest bright and dark exciton states, which is only[12] 100−250 μeV compared to the several meV energy separation in CdSe nanocrystals.[13] A smaller Δ_{BD} corresponds to a reduced phonon density of states for the phonon-assisted relaxation hence a longer spin−flip time. Such a behavior was clearly observed in the magnetic field dependence of the electron spin coherence in InGaAs QDs.[14] Δ_{BD} is tunable in QDs by controlling the electron−hole exchange interaction.[13] In practice, this is controlled by changing the size of the QD core ($\Delta_{BD} \propto 1/R^3$ in spherical dots of radius R) but also the extension of the wave function into the barrier since the electron−hole exchange depends on the extent of the electron−hole wave function overlap.[15] It was recently reported that, in CdSe/CdS colloidal QDs, which have a quasi-type-II band alignment corresponding to a delocalization of the electron wave function in the barrier material, a Δ_{BD} as low as 250 μeV is achieved on thick-shell samples.[16]

After understanding the physical origin of the ZPL exciton dephasing in CdSe QDs, we can expect to be able to control its time scale by engineering QDs with variable fine structure splitting Δ_{BD}. To verify this hypothesis, we have measured in this work the exciton dephasing in a series of quasi-type-II CdSe/CdS QDs with three different core diameters of 3.3, 4.6, and 5.7 nm and a CdS shell of 0, 2, or 9 monolayer (ML) thickness. We indeed find that the ZPL dephasing time at 5 K increases with increasing core size and shell thickness. Moreover, from the temperature dependence, we deduce Δ_{BD}, which correlates well with the measured dephasing, as expected from its physical origin.

RESULTS AND DISCUSSION

Transmission electron microscopy images showing CdSe/CdS QDs of the investigated sample series are given in Figure 1. X-ray diffraction patterns confirm that the crystal structure is zinc blende. Hence, the ~20 meV crystal-field splitting at the valence band maximum of the wurtzite crystal structure is *not* present in these QDs, an important point for their excitonic energy level structure, as will be discussed later

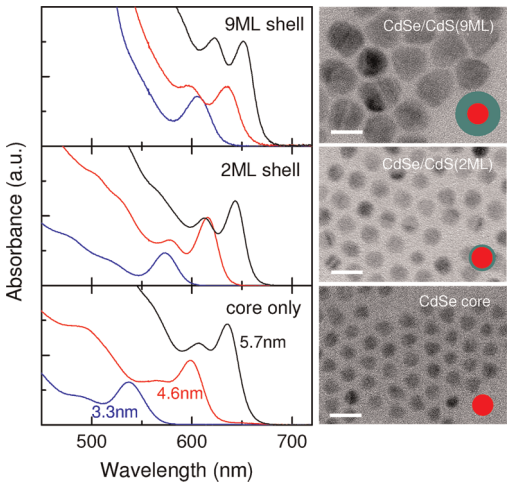

Figure 1. Left: Absorption spectra at room temperature of the synthesized CdSe/CdS QDs of different core diameters as indicated, having a 0, 2, or 9 ML shell thickness. Right: Transmission electron microscopy images of the corresponding samples with 4.6 nm core. Scale bar: 10 nm. Sketches of the core (red) and shell (green) structure are given for illustration.

(see also Supporting Information). The QDs are not perfectly spherical neither identical; that is, the ensemble is inhomogeneously broadened. Absorption spectra at room temperature (see Figure 1) of all investigated samples show the expected red shift of the ground-state excitonic absorption peak with increasing core size and shell thickness as a consequence of the reduced exciton localization. Measurements of the red shift by increasing the shell thickness layer-by-layer (see Supporting Information) indicate a saturation of the shift above 9 ML.

Similar to our previous work on CdSe/ZnS wurtzite QDs,[11] we have measured the dephasing time of the lowest bright exciton using transient three-beam FWM (see sketch in Figure 2) in resonance with the excitonic ground-state absorption. Each beam is a train of 150 fs pulses with 76 MHz repetition rate. The first pulse (P_1) induces a coherent polarization in the sample, which after a delay τ_{12} is converted into a density grating by the second pulse (P_2). The third pulse (P_3), delayed by τ_{23} from P_2, is diffracted by this density grating, yielding the FWM signal. In the heterodyne technique used,[17] the pulse trains are frequency shifted, resulting in a moving density grating and a frequency-shifted FWM field which is detected by its interference with an unshifted reference pulse of adjustable delay. In an inhomogeneously broadened ensemble, the FWM signal is a photon echo emitted at τ_{12} after P_3 and the microscopic dephasing is inferred from the decay of the photon echo amplitude *versus* τ_{12}. Conversely, the decay of the photon echo amplitude *versus* τ_{23} probes the exciton density dynamics.[18] The time-integrated FWM (TI-FWM) field amplitude *versus* τ_{12} given in Figure 2 is therefore a direct measure of the intrinsic exciton dephasing and shows systematic variations in

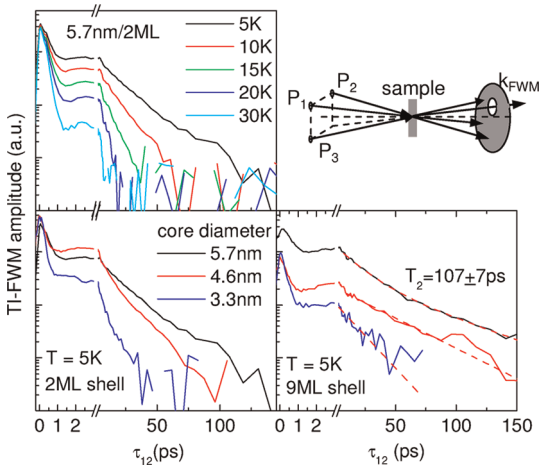

Figure 2. Measured time-integrated FWM field amplitude *versus* delay between the first two pulses for different temperatures for the 5.7 nm core 2 ML shell CdSe/CdS QDs (top left) and at 5 K for different samples (bottom), as indicated. The dashed lines are exponential fits to the data. The dephasing time inferred from the longest decay component in the 5.7 nm core 9 ML shell sample is also indicated. Top right is a sketch of the three-beam FWM directional geometry.

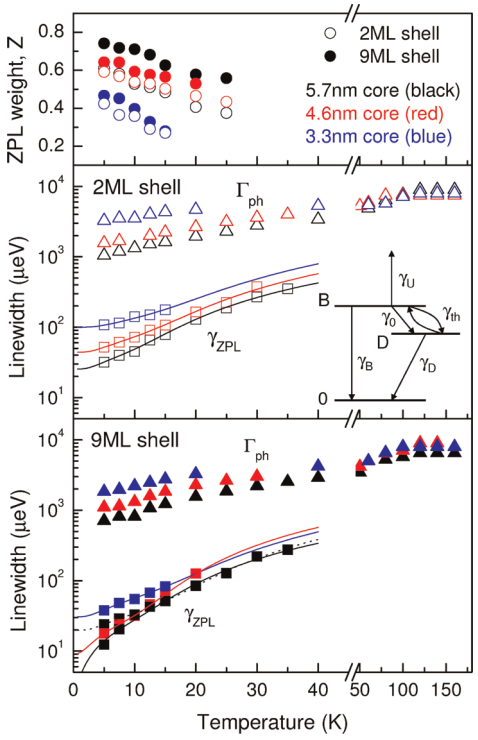

Figure 3. ZPL weight *Z* and homogeneous line width fwhm of the ZPL (γ_{ZPL}) and of the acoustic phonon band (Γ_{ph}) *versus* temperature in all investigated samples. The inset is a sketch of the lower bright−dark exciton relaxation model. The lines onto γ_{ZPL} are fits to the data (see text).

the investigated sample series. Generally, the dephasing has an initial subpicosecond component even at 5 K followed by a long exponential dephasing time (T_2) resolved at larger τ_{12}. This behavior reflects in time domain the composite homogeneous line shape consisting of a sharp Lorentzian ZPL (corresponding to the long exponential dephasing) superimposed onto a broad acoustic phonon band (the initial fast dephasing). It is due to the excitation of localized carriers, which distort the lattice equilibrium and couples the optical transition with phonon absorption/emission processes similar to roto-vibrational bands in molecules. We observe that with increasing dot diameter and shell thickness (*i.e.*, with decreasing localization) the initial component becomes slower and decreases its amplitude, which corresponds to a reduction of the acoustic phonon bandwidth and weight, respectively. Importantly, with decreasing localization, T_2 also increases, and we measure values at 5 K ranging from T_2 = 12 ps for the 3.3 nm core 2 ML shell sample to 41 ps for the 5.7 nm core 2 ML shell dots to even 107 ps as the longest decay for the 5.7 nm core 9 ML thick shell sample. With increasing temperature, the initial dephasing becomes faster and more dominant for all samples, as expected from the increased phonon occupation, while T_2 decreases (shown in Figure 2 for the 5.7 nm core 2 ML shell sample).

From the dynamics in Figure 2, we have quantified in Figure 3 the temperature dependence of the acoustic phonon band Γ_{ph} full width at half-maximum (fwhm) of the ZPL fwhm, $\gamma_{ZPL} = 2\hbar/T_2$, and of the ZPL weight, *Z*, using the method discussed in ref 8. Above 100 K, the initial dephasing becomes faster than the pulse duration in the experiment, hence the reported Γ_{ph} represents a lower bound. The dephasing at long delays is dominated by a monoexponential decay, hence a well-defined T_2 can be extracted. Only in the sample with 5.7 nm core and 9 ML shell is a significant biexponential decay observed, in which case the γ_{ZPL} values from both components are shown in Figure 3. We speculate that the biexponential decay is due to a larger (possibly bimodal) dot size distribution in this sample.

With decreasing exciton localization in the sample series, we observe that the ZPL weight increases and Γ_{ph} decreases, similar to what was shown in our previous work on InGaAs/GaAs QDs and as expected from theory within the so-called independent Boson model.[8] It is interesting to observe that, for the same core size, dots with thicker shell exhibit a larger ZPL weight and a smaller Γ_{ph}, indicating that the electron wave function localization plays an important role in the coupling with acoustic phonons. With increasing temperature, it is also expected that the weight of the ZPL decreases and the width of the phonon band increases,[8] which is indeed what we observe in all of our samples. With decreasing exciton localization, we also observe that γ_{ZPL} at 5 K decreases while showing a more rapid increase with temperature. To understand the temperature dependence of γ_{ZPL}, we have fitted the data following the same approach as in our previous work on CdSe/ZnS QDs[11] based on the

TABLE 1. Parameters Obtained from Fitting γ_{ZPL} *versus* Temperature: 5.7 nm/9 ML Lower and Upper Refer, Respectively, to Solid and Dashed Curves in Figure 3

	γ_0 (μeV)	Δ_{BD} (μeV)	γ_{0U} (meV)	Δ_U (meV)
3.3 nm/2 ML	100 ± 7	1200 ± 3000	3	7 ± 3
4.6 nm/2 ML	44 ± 2	820 ± 90	1.9 ± 0.8	6.3 ± 0.8
5.7 nm/2 ML	25 ± 1	680 ± 70	1.0 ± 0.2	5.2 ± 0.4
3.3 nm/9 ML	31 ± 4	680 ± 140	2.6	7.6 ± 0.8
4.6 nm/9 ML	9 ± 4	310 ± 190	2.2 ± 2.1	6 ± 1.6
5.7 nm/9 ML lower	2.9 ± 0.2	100	1.0 ± 0.4	5.7 ± 0.8
5.7 nm/9 ML upper	20 ± 2	750 ± 120	2.3 ± 0.6	7.6 ± 0.7

three-level model sketched in the inset of Figure 3. In this model, the dephasing rate is given by $\gamma_{ZPL} = \gamma_B + \gamma_0 + \gamma_{th} + \gamma_U$, where γ_B is the radiatively limited dephasing of the lowest bright state, γ_0 and γ_{th} are the spin−flip relaxation into the lowest dark state *via* spontaneous and stimulated phonon emission, respectively, and γ_U accounts for excitation into a higher state by phonon absorption. Hence $\gamma_{th} = \gamma_0 N_B$, where $N_B = 1/[\exp(\Delta_{BD}/k_BT) - 1]$ is the phonon occupation number, and similarly, $\gamma_U = \gamma_{0U}/[\exp(\Delta_U/k_BT) - 1]$. As will be shown later, the exciton density dynamics allows us to deduce γ_B, which is found to be negligible compared to γ_0 for all samples. Thus, the zero temperature extrapolated ZPL dephasing, $\gamma_0 + \gamma_B$, is dominated by the spin−flip rate, $\gamma_0 \gg \gamma_B$. Moreover, the increase of γ_{ZPL} with temperature up to about 20 K reflects the magnitude of Δ_{BD}. A summary of the parameters deduced from the fits of γ_{ZPL} *versus* temperature is shown in Table 1 (in some cases, to achieve convergence in the fit, not all parameters could vary freely, and those kept fixed are shown without errors).

Remarkably, there is a good correlation between γ_0 and Δ_{BD}, with the smallest γ_0 in the few μeV range for the smallest $\Delta_{BD} \sim 100$ μeV which, as expected, is found in dots with the largest core and thick shell. This correlation is consistent with our initial hypothesis that reducing Δ_{BD} reduces the spin−flip rate due to the reduced phonon density of states in the phonon-assisted relaxation.

To separately determine γ_B and gain more insight into the excitonic fine structure energy level scheme, we have investigated the temperature dependence of the exciton decay rate by measuring the TI-FWM *versus* τ_{23} and by time-resolved photoluminescence (PL) using time-correlated single-photon counting. TI-FWM *versus* τ_{23} is shown in Figure 4 on the 5.7 nm core 2 ML shell sample as an example. It exhibits a multiexponential decay which we fit with four time constants in the subpicosecond (τ_1), tens of picoseconds (τ_2), hundreds of picoseconds (τ_3), and few nanosecond (τ_4) range (data shown in Figure 4 are a zoom over the first 100 ps, but measurements were taken up to τ_{23} = 1.6 ns). The τ_1 and τ_2 are attributed to a subensemble of QDs resonantly excited in the upper bright states, showing a rapid relaxation toward the lower states,

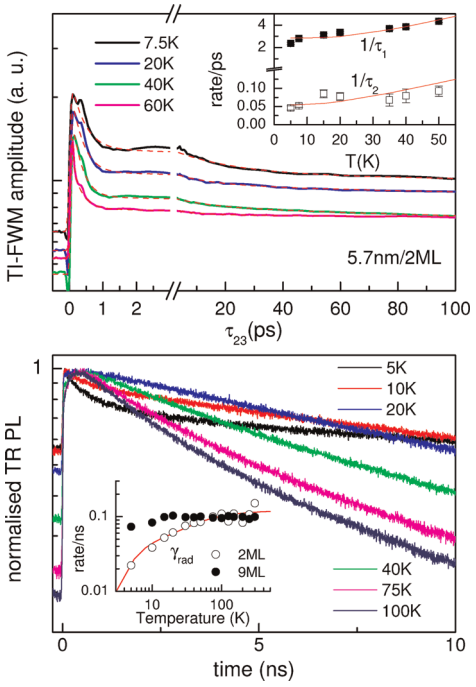

Figure 4. Top: Exciton density dynamics measured by TI-FWM *versus* τ_{23} at τ_{12} = 0 on the 5.7 nm core 2 ML shell sample. Dashed lines are fits to the data (see text). The inset shows the decay rates inferred from the first two time constants in the multiexponential dynamics and the corresponding temperature activated fits. Bottom: Time-resolved PL dynamics *versus* temperature on the same sample. The inset shows the exciton recombination rate deduced from the long exponential PL decay, together with the calculated thermal average of the radiative recombination within the excitonic fine structure. Filled symbols show the recombination rate for the 5.7 nm core 9 ML thick shell QDs.

which is expected considering the spectral width of the exciting pulses in the FWM experiment (~20 meV) and the inhomogeneous broadening in the sample (~70 meV). For a two-level system with a density dynamics determined by absorption and emission of phonons, the decay rate follows a thermally activated behavior given by $G[1 + 2/(\exp(\Delta/k_BT) - 1)]$, where Δ is the energy splitting between the two levels. Using this expression, we have fitted the temperature dependence of τ_1 and τ_2, as shown in the inset of Figure 4. An overview of the parameters obtained from these fits in the QDs with 5.7 and 4.6 nm core is shown in Table 2. For the 3.3 nm core samples, the first subpicosecond time constant is below the temporal resolution in the experiment, while the second time constant is found to be temperature-independent, indicating a large energy splitting ($\Delta > 10$ meV). We note that τ_1 is in the same time scale as the initial subpicosecond dephasing shown in Figure 2, hence it might contribute to it. This implies that the ZPL weight shown in Figure 3 is an underestimate. We find that the amplitude of the subpicosecond density decay is in the 30−50% range, nearly temperature-independent (see Figure 4), which corresponds to an underestimate of the ZPL weight of

TABLE 2. Parameters $G_{1,2}$ and $\Delta_{1,2}$ Obtained from the Fit of $\hbar/\tau_{1,2}$ with $\tau_{1,2}$ First Two Time Constants of the Exciton Density Decay Measured with FWM *versus* τ_{23}[a]

	G_1 (meV)	Δ_1 (meV)	G_2 (μeV)	Δ_2 (meV)
4.6 nm/2 ML	2.60 ± 0.04	9.4 ± 0.3	50 ± 5	7.1 ± 0.6
5.7 nm/2 ML	1.9 ± 0.1	6.5 ± 0.8	36 ± 8	4.5 ± 1.3
4.6 nm/9 ML	2.10 ± 0.05	4.8 ± 0.3		
5.7 nm/9 ML	1.67 ± 0.04	2.8 ± 0.1	30 ± 3	2.4 ± 0.4

[a] On the the 4.6 nm/9 ML sample, a good fit to the data was found using only τ_1.

10−15% from the cubic relationship[8] between the FWM field and *Z*.

Concerning the exciton dynamics at long delays, we found $\tau_3 \sim 400$ ps, which we attribute to Auger recombination of charged excitons,[19] and a τ_4 of several nanoseconds due to radiative recombination. Given the limited range of available delays in the FWM experiment, we have investigated the temperature-dependent radiative recombination rate using time-resolved PL, similar to what was shown in ref 20. PL measurements are shown in the bottom panel of Figure.4 for the 5.7 nm core 2 ML shell sample. At 5 K, the decay is biexponential (with a short, response-time-limited lifetime and a long lifetime[20]), which is a characteristic signature of the spin−flip relaxation of the bright exciton into the lowest dark level.[21] With increasing temperature, the decay becomes more monoexponential and represents the thermal average of the exciton radiative decay within the fine structure. The observation of a monoexponential decay already at 20 K suggests a dark−bright splitting of less than 2 meV, consistent with the FWM measurements (see Table 1). The temperature dependence of the rate γ_{rad} corresponding to the long decay component in the time-resolved PL is plotted in the bottom inset of Figure 4.

At this stage, let us discuss the excitonic energy fine structure in light of the results in Table 1 and Table 2 and of the temperature dependence of γ_{rad}. First we have calculated, following ref 13 (see also ref 20 and Supporting Information), the energy fine structure of nonperfectly spherical zinc blende core-only CdSe QDs to estimate the energy levels of the thin shell samples. Assuming a shape which retains cylindrical symmetry around an axis (*i.e.*, oblate or prolate), exciton levels are classified by the absolute value of the total angular momentum projection $|F|$ along this axis. It is this shape anisotropy that splits the lowest levels into an optically forbidden "dark" level ($|F| = 2$ two-fold degenerate in the oblate case, $F = 0$ called 0^L in the prolate case) energetically lying below a two-fold degenerate $|F| = 1$ bright level called $\pm1^L$, with an energy separation decreasing with increasing dot diameter and in the range of ~1 meV for 5 nm core diameter, consistent with our observations. Moreover, for slightly oblate QDs, three levels fairly close in energy to each other lie several meV above the $\pm1^L$, which are, in order of ascending separation from $\pm1^L$, the $F = 0$ called 0^L dark level, the $|F| = 1$ called $\pm1^U$ upper bright level, and the $F = 0$ called 0^U upper bright level. This ordering is consistent with the energy separations found in Table 1 and Table 2, with Δ_{BD} being the splitting between ±2 and $\pm1^L$, Δ_U being the average distance of $\pm1^L$ to the upper levels and $\Delta_{1,2}$ being the separations of $\pm1^L$ to the two upper bright levels. Within this picture, we have calculated γ_{rad} as the thermal average between these 5 sublevels, which is shown in Figure 4 for the 5.7 nm core 2 ML shell sample. We can well reproduce the measured temperature dependence using the energy separations from Table 1 and Table 2 and a radiative rate of the lowest bright state of 0.14 ± 0.02/ns, which corresponds to a radiatively limited dephasing of only $\gamma_B = 0.09 \pm 0.01$ μeV, much smaller than the spin−flip limited dephasing $\gamma_0 = 25$ μeV in this sample. The radiative rates of the upper bright states used to reproduce the experimental γ_{rad} are 0.32/ns for the 0^U level and 0.18/ns for the $\pm1^U$ level, scaling as expected from calculations of the oscillator strength for slightly oblate QDs (see Supporting Information). Similar results were found for the other thin shell samples. Moreover, with increasing shell thickness, we found a much reduced temperature dependence of γ_{rad} (see bottom inset Figure 4 for the 5.7 nm core 9 ML shell sample) which is consistent with the reduced fine structure splitting in these dots.

A final confirmation that the ZPL dephasing of the lowest bright exciton at low temperature originates from spin−flip relaxation is obtained from a direct measurement of the bright−dark relaxation in our samples *via* the FWM amplitude *versus* τ_{23} for $\tau_{12} > 0$. As shown in our previous work on CdSe/ZnS QDs,[11] this measurement is sensitive to the density dynamics within the fine structure since a spectrally modulated density grating is created. In Figure 5 (left), the measured FWM amplitude *versus* τ_{23} at 10 K is shown for three different values of τ_{12} for the 5.7 nm core 2 ML shell sample. We clearly observe that for $\tau_{12} > 0$ a new initial dynamics appears, the effect being most pronounced for $\tau_{12} = 1$ ps. As explained in our previous work,[11] we expect the bright−dark relaxation to manifest as an additional decrease in the FWM signal *versus* τ_{23}. Moreover, due to the phase difference between the fields from the crystal ground state to exciton transition and exciton−biexiton transition at the photon echo time, this decrease is most pronounced for τ_{12} equal to half the exciton−biexciton beat period.[11] In Figure 5 (left), we show also the ratio between the FWM dynamics at $\tau_{12} = 1$ ps and $\tau_{12} = 0$ to highlight the presence of the new time constant (τ_s) which we infer with an exponential decay fit. This time constant is in good agreement with the measured ZPL dephasing time taken as a density lifetime $T_2/2$, as shown in Figure 5 (right). One should also note that τ_s is

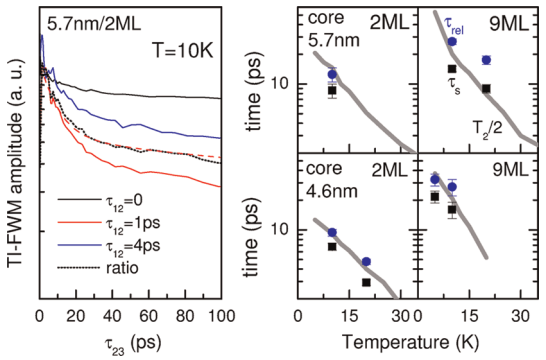

Figure 5. Left: TI-FWM field amplitude *versus* τ_{23} for different τ_{12} for the 5.7 nm core 2 ML shell sample at 10 K. The ratio between the dynamics at τ_{12} = 1 ps and the dynamics at τ_{12} = 0 is also shown (dotted line) together with its fit (dashed line). Right: Additional time constant τ_s (squares) inferred from the dynamics at $\tau_{12} \neq 0$ is compared with the measured ZPL dephasing time on different samples as indicated. The relaxation time constant τ_{rel} deduced from τ_s is also shown (see text).

the thermalization time between the bright and dark states. In the low-temperature limit, where the spin−flip relaxation time into the lowest dark state is the dominant dephasing mechanism (*i.e.*, higher dark states can be neglected), one can relate τ_s to the dephasing using a simple two-level system description. In this case, the rate $1/\tau_s$ is the sum of phonon-assisted absorption and emission (spontaneous plus stimulated) rates between the lowest bright and dark states, while the dephasing is given only by the relaxation (hence emission) rate. Thus the time constant to be compared with $T_2/2$ is not exactly τ_s but the relaxation time $\tau_{rel} = \tau_s[1 + \exp(-\Delta_{BD}/k_BT)]$. In Figure 5 (right), both τ_{rel} and τ_s are shown for the 5.7 nm core and 4.6 nm core samples (where the signal-to-noise ratio in the measurements was sufficient to perform this analysis), and we see that τ_{rel} is indeed in very good agreement with the dephasing time at low temperature.

CONCLUSION

In conclusion, we have shown that the intrinsic zero-phonon line dephasing of the ground-state exciton in quasi-type-II CdSe/CdS zinc blende colloidal quantum dots at low temperatures is due to the spin−flip from the lowest bright to the dark exciton state. Importantly, this dephasing is tuned by engineering the excitonic fine structure, which is achieved in our sample series by varying the core size and shell thickness and in turn the electron−hole exchange interaction. We find that by decreasing the bright-dark energy splitting Δ_{BD} the zero-temperature extrapolated dephasing rate, and in turn the homogeneous line width, decreases to values as low as ∼3 μeV for $\Delta_{BD} \sim 100$ μeV. It should be emphasized that the use of quasi-type-II dots enables wave function engineering beyond mere size tuning, with the potential to extend the dephasing time at any predefined wavelength. The ability to tailor the exciton dephasing time demonstrated in this work is a key step toward the exploitation of colloidal quantum dots for coherent quantum dynamics applications.

METHODS

Synthesis and Structural Characterization. Colloidal CdSe core QDs were synthesized according to an established procedure.[22] The CdS shell was grown by succesive ion layer addition and reaction (SILAR).[23] With the QD diameter and concentration, we calculated the amount of Cd and S to be added to form a shell of 2 and 9 monolayers, respectively. For all samples, the average core diameter and shell thickness were determined using transmission electron microscopy by measuring the average diameter of the CdSe core-only QDs and the corresponding CdSe/CdS core−shell QDs. The resulting shell thickness agrees with the predetermined number of layers using a thickness of 0.34 nm per CdS monolayer.

Transient FWM Measurements. Colloidal QDs were dispersed in a polystyrene film and sandwiched between two quartz windows mounted onto a coldfinger cryostat for temperature-dependent measurements. To preferentially excite the lowest bright ground-state excitonic absorption, the center wavelength of the exciting pulses was tuned below the PL emission at low temperature by an amount on the order of the Stokes shift in these QDs. To minimize selective excitation of linearly polarized transitions in the ensemble of randomly oriented colloidal QDs, all pulses were co-circularly polarized. Transient FWM measurements *versus* τ_{12} were taken for nonzero $\tau_{23} = 1$ ps to exclude nonresonant nonlinearities. The time-averaged excitation intensity was well within the third-order nonlinear regime and also resulted in negligible local heating as we affirmed by power-dependent measurements.

Time-Resolved PL Measurements. QDs were drop-cast on a quartz glass plate, forming a close-packed thin film. Samples were mounted in a helium cryostat for time-resolved PL measurements in a temperature range of 5−300 K. QDs were excited at 400 nm (*i.e.*, far above the band gap) by a frequency-doubled 80 MHz Ti:Sa femtosecond pulsed laser. PL traces were collected by time-correlated single-photon counting using an avalanche photodiode.

Conflict of Interest: The authors declare no competing financial interest.

Acknowledgment. Rainer F. Mahrt and Gabriele Rainò (IBM Research-Zürich) are acknowledged for stimulating discussions. P.B. is a Leadership fellow of the EPSRC UK Research Council (Grant No. EP/I005072/1). Z.H. acknowledges BelSPo (IAP 6.10, Photonics@be) and the FWO-Vlaanderen (grant no. G.0794.10) for funding this research.

Supporting Information Available: Measurements of band gap shift with increasing shell thickness. Fine structure calculations. This material is available free of charge *via* the Internet at http://pubs.acs.org.

REFERENCES AND NOTES

1. Henneberger, F., Benson, O., Eds. *Semiconductor Quantum Bits*; Pan Stanford Publishing: Portland, OR, 2009.
2. Kasprzak, J.; Reitzenstein, S.; Muljarov, E. A.; Kistner, C.; Schneider, C.; Strauss, M.; Höfling, S.; Forchel, A.; Langbein, W. Up on the Jaynes-Cummings Ladder of a Quantum-Dot/Microcavity System. *Nat. Mater.* **2010**, *9*, 304–308.
3. Wiersig, J.; Gies, C.; Jahnke, F.; Assmann, M.; Berstermann, T.; Bayer, M.; Kistner, C.; Reitzenstein, S.; Schneider, C.; Höfling, S.; Forchel, A.; Kruse, C.; Kalden, J.; Hommel, D. Direct Observation of Correlations between Individual

Photon Emission Events of a Microcavity Laser. *Nature* **2009**, *460*, 245–249.
4. Yin, Y.; Alivisatos, A. P. Colloidal Nanocrystal Synthesis and the Organic Inorganic Interface. *Nature* **2005**, *437*, 664–670.
5. Borri, P.; Langbein, W.; Schneider, S.; Woggon, U.; Sellin, R. L.; Ouyang, D.; Bimberg, D. Ultralong Dephasing Time in InGaAs Quantum Dots. *Phys. Rev. Lett.* **2001**, *87*, 157401.
6. Birkedal, D.; Leosson, K.; Hvam, J. M. Long Lived Coherence in Self-Assembled Quantum Dots. *Phys. Rev. Lett.* **2001**, *87*, 227401.
7. Langbein, W.; Borri, P.; Woggon, U.; Stavarache, V.; Reuter, D.; Wieck, A. D. Radiatively Limited Dephasing in InAs Quantum Dots. *Phys. Rev. B* **2004**, *70*, 033301.
8. Borri, P.; Langbein, W.; Woggon, U.; Stavarache, V.; Reuter, D.; Wieck, A. Exciton Dephasing *via* Phonon Interactions in InAs Quantum Dots: Dependence on Quantum Confinement. *Phys. Rev. B* **2005**, *71*, 115328.
9. Palinginis, P.; Tavenner, S.; Lonergan, M.; Wang, H. Spectral Hole Burning and Zero Phonon Linewidth in Semiconductor Nanocrystals. *Phys. Rev. B* **2003**, *67*, 201307.
10. Biadala, L.; Louyer, Y.; Tamarat, P.; Lounis, B. Direct Observation of the Two Lowest Exciton Zero-Phonon Lines in Single CdSe/ZnS Nanocrystals. *Phys. Rev. Lett.* **2009**, *103*, 037404.
11. Masia, F; Accanto, N.; Langbein, W.; Borri, P. Spin−Flip Limited Exciton Dephasing in CdSe/ZnS Colloidal Quantum Dots. *Phys. Rev. Lett.* **2012**, *108*, 087401.
12. Bayer, M.; Ortner, G.; Stern, O.; Kuther, A.; Gorbunov, A. A.; Forchel, A.; Hawrylak, P.; Fafard, S.; Hinzer, K.; Reinecke, T. L.; Walck, S. N.; Reithmaier, J. P.; Klopf, F.; Schäfer, F. Fine Structure of Neutral and Charged Excitons in Self-Assembled In(Ga)As/(Al)GaAs Quantum Dots. *Phys. Rev. B* **2002**, *65*, 195315.
13. Efros, A.; Rosen, M.; Kuno, M.; Nirmal, M.; Norris, D.; Bawendi, M. Band Edge Exciton in Quantum Dots of Semiconductors with a Degenerate Valence Band: Dark and Bright Exciton States. *Phys. Rev. B* **1996**, *54*, 4843–4856.
14. Kroutvar, M.; Ducommun, Y.; Heiss, D.; Bichler, M.; Schuh, D.; Abstreiter, G.; Finley, J. Optically Programmable Electron Spin Memory Using Semiconductor Quantum Dots. *Nature* **2004**, *432*, 81–84.
15. He, J.; Zhong, H.; Scholes, G. D. Electron−Hole Overlap Dictates the Hole Spin Relaxation Rate in Nanocrystal Heterostructures. *Phys. Rev. Lett.* **2010**, *105*, 046601.
16. Brovelli, S.; Schaller, R.; Crooker, S.; García-Santamaria, F.; Chen, Y.; Viswanatha, R.; Hollingsworth, J.; Htoon, H.; Klimov, V. Nano-Engineered Electron−Hole Exchange Interaction Controls Exciton Dynamics in Core−Shell Semiconductor Nanocrystals. *Nat. Commun.* **2011**, *2*, 208.
17. Borri, P.; Langbein, W. Four-Wave Mixing Dynamics of Excitons in InGaAs Self-Assembled Quantum Dots. *J. Phys.: Condens. Matter* **2007**, *19*, 295201.
18. Shah, J. *Ultrafast Spectroscopy of Semiconductors and Semiconductor Nanostructures*; Springer: Berlin, 1996.
19. Klimov, V. I.; Mikhailovsky, A. A.; McBranch, D. W.; Leatherdale, C. A.; Bawendi, M. G. Quantization of Multiparticle Auger Rates in Semiconductor Quantum Dots. *Science* **2000**, *287*, 1011–1013.
20. Moreels, I.; Rainò, G.; Gomes, R.; Hens, Z.; Stöferle, T.; Mahrt, R. F. Band-Edge Exciton Fine Structure of Small, Nearly Spherical Colloidal CdSe/ZnS Quantum Dots. *ACS Nano* **2011**, *5*, 8033–8039.
21. Labeau, O.; Tamarat, P.; Lounis, B. Temperature Dependence of the Luminescence Lifetime of Single CdSe/ZnS Quantum Dots. *Phys. Rev. Lett.* **2003**, *90*, 257404.
22. Jasieniak, J.; Bullen, C.; van Embden, J.; Mulvaney, P. Phosphine-Free Synthesis of CdSe Nanocrystals. *J. Phys. Chem. B* **2005**, *109*, 20665–20668.
23. Li, J. J.; Wang, Y. A.; Guo, W. Z.; Keay, J. C.; Mishima, T. D.; Johnson, M. B.; Peng, X. G. Large Scale Synthesis of Nearly Monodisperse CdSe/CdS Core/Shell Nanocrystals Using Air-Stable Reagents *via* Successive Ion Layer Adsorption and Reaction. *J. Am. Chem. Soc.* **2003**, *125*, 12567–12575.